RAA 2021 Vol. **21** No. **7**, 162(13pp) doi: 10.1088/1674-4527/21/7/162

http://www.raa-journal.org *http://iopscience.iop.org/raa*

***R**esearch in*
***A**stronomy and*
***A**strophysics*

A relativistic model of stellar objects with core-crust-envelope division

Ravindra K. Bisht[1], Satyanarayana Gedela[1,2], Neeraj Pant[1] and Neeraj Tewari[3]

[1] Department of Mathematics, National Defence Academy, Khadakwasla, Pune - 411023, India; *ravindra.bisht@yahoo.com, satya235@gmail.com, neeraj.pant@yahoo.com*
[2] Department of Mathematics, SSJ Campus, Kumaun University, Almora - 263601, India
[3] Department of Physics, Lajpat Rai College, Ghaziabad - 201005, India; *neerajtewari.ntl@gmail.com*

Received 2021 January 7; accepted 2021 February 7

Abstract In this work, we present a cogent and physically well-behaved solution for neutron stars envisaged with a core layer having quark matter satisfying the MIT-bag equation of state (EoS), meso layer with Bose-Einstein condensate (BEC) matter satisfying modified BEC EoS and an envelope having neutron fluid and Coulomb liquids satisfying quadratic EoS. All the required physical and geometrical parameters like gravitational potentials, pressures, radial velocity, anisotropy, adiabatic index, mass function, compactification factor, and gravitational and surface redshift functions show a feasible trend and are continuous with smooth variation throughout the interior and across the regions of the star. Further, causality condition, energy conditions, static stability criterion (using Tolman-Oppenheimer-Volkoff equation) and Herrera cracking stability criterion are met throughout the star. The approach seems to be resulting in more realistic and accurate modeling of stellar objects, particularly realized by us for X-ray binary stars 4U 1608–52 ($M = 1.7\,M_{\odot}$, $R = 9.5$ km) and SAX J1808.4–3658 ($M = 1.2\,M_{\odot}$, $R = 7.2$ km). Furthermore, we have ascertained that the continuity of the stability factor in all three regions of the stars demand a smaller core. As the core region of the star increases, the stability factor becomes discontinuous at all the interfaces inside the star.

Key words: stars: interiors — stars: neutron — Galaxy: stellar content

1 INTRODUCTION

Neutron stars are stellar residues left after supernova explosions. Due to the unavailability of an Earth based laboratory, the comprehensive description of neutron stars may be useful to grasp the nature of four fundamental forces, i.e., gravitational, electromagnetic, weak and strong force under extreme conditions. Despite having an ultra-dense matter distribution and gravity, stellar objects still exist with a staggering amount of composite structure.

The atmospheres of these objects starting from the surface and beyond are composed mostly of hydrogen and helium. The outer crust, with a thickness of a few hundred meters, contains atomic nuclei and free electrons, while the inner crust, a very dense solid layer, is made of free neutrons and electrons as well as heavier atomic nuclei. The next layer is an outer core, having a neutron-rich quantum liquid. Finally, at the innermost part the strong force, responsible for the fundamental interaction between quarks in nucleons, paves the way to the inner core, a mysterious but ultra-dense type of matter in the discernible cosmos (Mann 2020; Potekhin 2010; Heiselberg 2001; Heiselberg & Hjorth-Jensen 2000; Lattimer & Prakash 2004; Baym & Pethick. 1979).

One of the groundbreaking earlier works on interior structures of neutron stars is credited to Ginzberg (1971). Many researchers have hypothesized the possibility of different matter compositions inside neutron stars comprising several layers including the inner and outer cores, inner and outer crusts, mantle, ocean, envelope and atmosphere. The core may contain quark matter, quark-gluon plasma (QGP) besides witnessing the phenomena of hyperonization, pion and/or kaon condensation. A plasma envelope may be made up predominantly of neutron fluid, atoms and/or Coulomb liquids (Ruderman 1968; Ginzburg 1969; Migdal 1960; Glendenning 1992; Alford 2001; Bedaque et al. 2002; Pisalski & Wilczek 1984).

The possibility of a quark core is due to the stability of quark phase over hadronic phase at the interior of a compact star (Witten 1984; Farhi & Jaffe 1984). Authors (Cheng et al. 1998; Ketter et al. 1995; Phukon 2000) have

suggested that strange stars have a low density nuclear crust with a thin electron layer between crust and core. Colpi et al. (1986) predicted that the quark-diquark core is wrapped by a low density nucleon envelope. The idea of a deconfined quark core inside a low density mixed phase envelope was presented by Drago & Lavagno (2001). Chavanis & Harko (2012) examined a tentative insight that due to their superfluid properties some compact stars may comprise a substantial amount of their matter in the form of a Bose-Einstein condensate (BEC). However, the prospect of the existence of some BECs in neutron stars was mooted by Glendenning (2000). The role of BEC in kaons/anti-kaons in compact objects was studied in Banik & Bandyopadhyay (2003) and Banik et al. (2004). Kapusta (2004) emphasized that neutrino superfluidity may also contribute to BEC in the study of complex structure of compact objects (see also Abuki 2007).

Multi-layer structures of neutron or strange stars have invigorated various researches to inquire into core-envelope or two layer modeling in the setting of general relativity. In this model, the core and envelope are assumed to be individually satisfying distinct equations of state (EoSs) and/or gravitational metric potential(s). At last, the interfaces are matched applying the Dormois-Israel condition to ascertain the continuity of all the physical parameters. The first core-envelope model was proposed by Bondi (1964) with an EoS $p = \rho/3$. Afterwards, many authors (Das & Narlikar 1975; Vaidya & Tikekar 1982; Sharma & Mukherjee 2001, 2002; Usmani 2011; Rahaman et al. 2012a,b; Chan et al. 2011; Durgapal & Gehlot 1969, 1971; Paul & Tikekar 2005; Tikekar & Thomas 2005; Thomas et al. 2005; Tikekar & Jotania 2009; Takisa & Maharaj 2016; Hansraj et al. 2016; Singh et al. 2020a,b) studied core-envelope solutions for the Einstein field equations by assuming different EoSs. It is a painstaking task to consider realistic EoSs for poly-layered stellar objects. The generally used EoSs for core – envelope models of a neutron star include linear EoS with MIT bag model (Sharma & Maharaj 2007; Takisa & Maharaj 2013a; Thirukkanesh & Ragel 2013; Takisa et al. 2014b; Maurya et al. 2019; Esculpi & Alom 2010; Bhar et al. 2015); quadratic EoS (Feroze & Siddiqui 2011; Maharaj & Takisa 2012; Takisa et al. 2014a; Bhar et al. 2016, 2017; Sunzu & Thomas 2018; Govender et al. 2017, 2019; Gedela et al. 2019); polytropic EoS (Ngubelanga & Maharaj 2017; Noureen et al. 2019; Takisa & Maharaj 2013b); Van der Waals EoS (Thirukkanesh et al. 2014) and Chaplygin's EoS (Bhar et al. 2018; Benaoum 2002; Rahaman et al. 2010).

Takisa et al. (2019) studied a core-envelope model with the core layer having a quark matter distribution and envelope consisting of matter distribution endowed with linear and quadratic EoSs, respectively. Pant et al. (2019) and Gedela et al. (2019) also studied core-envelope stellar models of various stars and successfully verified continuity of most of the physical parameters except stability factor, transverse pressure and velocity at the junction of the core and envelope.

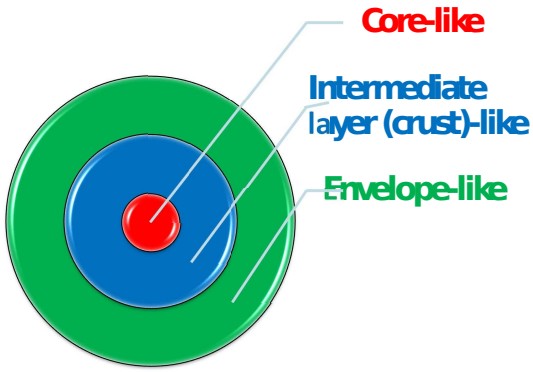

Fig. 1 Three layered relativistic model of X-ray binary star 4U 1608–52.

Motivated by various two layer models, Pant et al. (2020) proposed a three layered relativistic hybrid star model in the setting of general relativity. In order to make the model, an intermediate layer was sandwiched between the core and envelope which paved the way to understand neutron star modeling in a more realistic and accurate way. In Pant et al. (2020), the authors also verified continuity of some of the physical parameters at the junctions of all the three interfaces. Due to the discontinuous nature of stability factor, transverse pressure and velocity at each of the interfaces, these conditions were not studied by Pant et al. (2020). In this paper, we construct a more realistic and accurate model of stellar objects, particularly X-ray binary stars 4U 1608–52 ($M = 1.7\,M_{\odot}$, $R = 9.5$ km) and SAX J1808.4–3658 ($M = 1.2\,M_{\odot}$, $R = 7.2$ km). In addition, we have realized that continuity of the stability factor in all three regions of the star SAX J1808.4–3658 demands a smaller core. As the core region of the star increases, the stability factor becomes discontinuous at all the interfaces inside of the star. Following the article of Pant et al. (2020), we slightly modify the nomenclature of three regions with three distinct EoSs of a three layered hybrid star model as follows (see Fig. 1):

(i) Quark core-like inner region with MIT-bag EoS;
(ii) Crust like intermediate region with modified BEC EoS;
(iii) Envelope-like region with quadratic EoS.

Corresponding to the above defined three regions of this hybrid star model, three interfaces, namely, core-intermediate layer interface, intermediate layer-envelope interface and envelope-boundary interface are considered

and using Dormois-Israel conditions all three interfaces are required to match for continuity of all the physical parameters. Our proposed model affirms that all the physical and geometrical parameters have viable trend and values. Further, these parameters are continuous with smooth variations throughout the star's interior resulting in a more realistic and accurate modeling of stellar objects. We propose relativistic three layer models of X-ray binary star 4U 1608–52 and SAX J1808.4–3658 (Gangopadhya et al. 2013) and discuss their behaviors through graphical representations and in the form of tables.

2 EINSTEIN FIELD EQUATIONS IN THREE LAYERED MODEL

We consider the most general form of a static spatially spherically symmetric line element for the interior space-time as

$$ds^2 = e^{\nu}dt^2 - e^{\lambda}dr^2 - r^2(d\theta^2 + \sin^2\theta d\phi^2), \quad (1)$$

where ν and λ are some unknown functions of the radial coordinate r to be determined.

We assume an anisotropic matter distribution inside the fluid sphere and the energy-momentum tensor is considered as

$$T^i_j = [(p_t + \rho)v^i v_j - p_t g^i_j + (p_r - p_t)\chi^i\chi_j], \quad (2)$$

where ρ, p_r and p_t are energy density, radial pressure appraised in the direction of the space-like vector and transverse pressure in the orthogonal direction to p_r, respectively. In co-moving coordinates, v^i is the normalized 4-velocity and χ^j is the unit space-like vector in the radial direction.

Utilizing energy momentum tensor (2), the Einstein field equations (with the units $G = c = 1$) can be written as

$$8\pi\rho = \frac{\left(1 - e^{-\lambda}\right)}{r^2} + \frac{\dot{\lambda}e^{-\lambda}}{r}, \quad (3)$$

$$8\pi p_r = \frac{\dot{\nu}e^{-\lambda}}{r} - \frac{\left(1 - e^{-\lambda}\right)}{r^2}, \quad (4)$$

$$8\pi p_t = \frac{e^{-\lambda}}{4}\left(2\ddot{\nu} + \dot{\nu}^2 - \dot{\nu}\dot{\lambda} + \frac{2\dot{\nu}}{r} - \frac{2\dot{\lambda}}{r}\right), \quad (5)$$

where "˙" denotes derivative with respect to the radial coordinate r.

Recently, Herrera (2020) observed the fact that physical processes obtained in the study of stellar evolution always tend to produce pressure anisotropy, even if the system is initially assumed to be isotropic. The initial isotropic configuration may lead to local anisotropic pressure due to shear flow, dissipative fluxes and inhomogeneities in energy-density during dissipative downfall. However, the magnitude of the attained pressure anisotropy would rely on the specific characteristics of the system. In fact, in any equilibrium configuration which is the final stage of a dynamic regime, the acquired anisotropy during this dynamic process does not disappear in the final equilibrium state, and therefore the resulting configuration, even if initially having isotropic pressure, should in principle exhibit pressure anisotropy. The measure of anisotropy (Δ) of the fluid sphere can be calculated as

$$\Delta = 8\pi(p_t - p_r). \quad (6)$$

Considering the transformations $x = r^2$, $z(x) = e^{-\lambda(r)}$ and $y(x) = e^{\nu(r)}$, the field Equations (3)–(6) take the forms

$$8\pi\rho = \frac{1 - z}{x} - 2z', \quad (7)$$

$$8\pi p_r = 2z\frac{y'}{y} - \frac{1 - z}{x}, \quad (8)$$

$$8\pi p_t = z\left[\left(\frac{2y''}{y} - \frac{y'^2}{y^2}\right)x + \frac{2y'}{y}\right] + z'\left(1 + x\frac{y'}{y}\right), \quad (9)$$

$$8\pi\Delta = z\left(\frac{2y''}{y} - \frac{y'^2}{y^2}\right)x + z'\left(1 + x\frac{y'}{y}\right) + \frac{1 - z}{x}, \quad (10)$$

where $(')$ and $('')$ represent first and second derivatives with respect to x respectively.

In order to make a three layered model for relativistic stellar objects, it is mandatory to classify space-time into three layers comprised of the core layer $(0 \le r \le R_c)$, intermediate layer $(R_c \le r \le R_i)$ and envelope layer $(R_i \le r \le R_e)$. We now consider the following three line elements corresponding to the above defined three layers as

$$ds^2|_c = e^{\nu_c(r)}dt^2 - e^{\lambda_c(r)}dr^2 - r^2(d\theta^2 + \sin^2\theta d\phi^2), \quad (11)$$

$$ds^2|_i = e^{\nu_i(r)}dt^2 - e^{\lambda_i(r)}dr^2 - r^2(d\theta^2 + \sin^2\theta d\phi^2), \quad (12)$$

$$ds^2|_e = e^{\nu_e(r)}dt^2 - e^{\lambda_e(r)}dr^2 - r^2(d\theta^2 + \sin^2\theta d\phi^2). \quad (13)$$

3 FORMULATION OF CORE-INTERMEDIATE-ENVELOPE-LIKE LAYERS

Henceforth, letters in lower script *c*, *i* and *e* correspond to the core, meso or intermediate layer and envelope, respectively of a relativistic star model.

3.1 Core-like Layer Having Quark Matter Satisfying MIT-bag EoS

For the core layer ($0 \leq r \leq R_c$), we select the same g_{rr} as in Gedela et al. (2019) for e^{λ} satisfying the MIT-bag EoS

$$z = e^{-\lambda_c} = 1 + \frac{sx}{(tx+1)^2}, \tag{14}$$

$$p_{r_c} = a\rho - b, \tag{15}$$

where $s,\ t,\ a$ and b are constants. Using Equations (7), (8), (10), (14) and (15), we get

$$\frac{y'(x)}{y(x)} + \left(\frac{s(a(3-tx)+tx+1)}{tx+1} + \frac{4\pi b(tx+1)^2}{sx+(tx+1)^2} \right) = 0. \tag{16}$$

On integration (16), we obtain

$$\begin{aligned} y &= e^{\nu_c} \\ &= C_1 d_2 e^{\left(\frac{\sqrt{s} d_1 \tanh^{-1}(d_0)}{t^2\sqrt{s+4t}} - 4\pi b x \right)}, \end{aligned} \tag{17}$$

where C_1 is an integration constant. Applying the transformation $x = r^2$ and (14) and (17), the physical variables (7)-(10) become

$$\rho_c = \frac{s\left(r^2 t - 3\right)}{8\pi\left(r^2 t + 1\right)^3}, \tag{18}$$

$$p_{r_c} = \frac{as\left(r^2 t - 3\right)}{8\pi\left(r^2 t + 1\right)^3} - b, \tag{19}$$

$$p_{t_c} = \frac{d_3 + r^2 s\left(d_4 s + d_5\right) - 16\pi b d_6\left(r^2 t + 1\right)^3}{32\pi\left(r^2 t + 1\right)^4\left(r^2 s + \left(r^2 t + 1\right)^2\right)}, \tag{20}$$

$$\Delta_c = p_{t_c} - p_{r_c}, \tag{21}$$

where

$$\begin{aligned} d_0 &= \frac{s + 2t(tx+1)}{\sqrt{s}\sqrt{s+4t}}, \\ d_1 &= \left((a+1)t^2 + 4\pi b(s+2t)\right), \\ d_2 &= (tx+1)^{2a}\left(sx + (tx+1)^2\right)^{\frac{2\pi b s}{t^2} - a}, \\ d_3 &= 64\pi^2 b^2 r^2\left(r^2 t + 1\right)^6 - 12as, \\ d_4 &= 9a^2 + ((a-4)a - 1)r^4 t^2 \\ &\quad + 2(a(14-3a)+1)r^2 t + 3, \\ d_5 &= 4at\left(r^2 t\left(r^2 t\left(6 - r^2 t\right) + 12\right) + 2\right), \\ d_6 &= r^2\left(as\left(r^2 t - 3\right)\right. \\ &\quad \left. + 2t\left(r^2\left(t\left(r^2 t + 3\right) + s\right) + 3\right)\right) + 2. \end{aligned}$$

With the help of the transformation $x = r^2$, the physical parameters mass $m_c(r)$, compactification factor ($u_c(r)$), gravitational redshift ($z_{g_c}(r)$) and surface redshift ($z_{s_c}(r)$) for the core layer ($0 \leq r \leq R_c$) can be obtained from the following expressions:

$$m_c(r) = 4\pi \int r^2 \rho_c dr = -\frac{r^3 s}{2\left(r^2 t + 1\right)^2}, \tag{22}$$

$$u_c(r) = \frac{m_c(r)}{r} = -\frac{r^2 s}{2\left(r^2 t + 1\right)^2}, \tag{23}$$

$$z_{g_c}(r) = e^{-\nu_c/2} - 1, \tag{24}$$

$$z_{s_c}(r) = \frac{1}{\sqrt{1 - 2u_c(r)}} - 1. \tag{25}$$

3.2 Intermediate Layer having BEC Matter Satisfying Modified BEC EoS

For intermediate layer ($R_c \leq r \leq R_e$), we select the same metric potential g_{rr} as assumed in the core layer satisfying a modified BEC EoS (the classical BEC EoS has the form $p \propto \rho^2$)

$$z = e^{-\lambda_i} = 1 + \frac{sx}{(tx+1)^2}, \tag{26}$$

$$p_{r_i} = d\rho^2 - f, \tag{27}$$

where $s,\ t,\ d$ and f are constants. Utilizing Equations (7), (8), (10), (26) and (27), we obtain

$$\frac{y'(x)}{y(x)} + \frac{s + 8\pi(tx+1)^2}{2\left(sx + (tx+1)^2\right)} = \frac{ds^2(tx-3)^2}{16\pi(tx+1)^4\left(sx + (tx+1)^2\right)}. \tag{28}$$

On integrating (28), we get

$$y_i = e^{\nu_i} = C_2 \exp\left(\frac{d_7 \tanh^{-1}(d_0) + d_6}{16\pi} \right), \tag{29}$$

where C_2 is an integration constant.

With the help of Equations (26) and (29) and the transformation $x = r^2$, the field Equations (7)-(10) can be written as

$$\rho_i = \frac{s\left(r^2 t - 3\right)}{8\pi\left(r^2 t + 1\right)^3}, \tag{30}$$

$$p_{r_i} = \frac{ds^2\left(r^2 t - 3\right)^2}{64\pi^2\left(r^2 t + 1\right)^6} - f, \tag{31}$$

$$p_{t_i} = \frac{-128\pi^2 d_{10} f\left(r^2 t + 1\right)^6 + \left(d_8 - d_9\right)s^2\left(r^2 t - 3\right)}{2048\pi^3\left(r^2 t + 1\right)^{10}\left(r^2 s + \left(r^2 t + 1\right)^2\right)} + \frac{d_{11}}{2048\pi^3\left(r^2 t + 1\right)^{10}\left(r^2 s + \left(r^2 t + 1\right)^2\right)}, \tag{32}$$

$$\Delta_i = p_{t_i} - p_{r_i}, \tag{33}$$

where

$$d_6 = \frac{\left(3dt^2(3s+8t)+64\pi^2 fs\right)\log\left(sx+(tx+1)^2\right)}{2t^2} + \frac{d\left(s(3tx(9tx+22)+55)+48t(tx+1)^2\right)}{3(tx+1)^3} - 3d(3s+8t)\log(tx+1) - 64\pi^2 fx\,,$$

$$d_7 = \frac{64\pi^2 fs(s+2t)}{t^2\sqrt{s(s+4t)}} - \frac{t^2\left(9ds^2+42dst+32dt^2-16\pi s\right)}{t^2\sqrt{s(s+4t)}}\,,$$

$$d_8 = d^2r^2s^2\left(r^2t-3\right)^3 - 64\pi^2r^2\left(r^2t+1\right)^7\,,$$

$$d_9 = 32\pi d\left(r^2t+1\right)^3\left(3+r^2t\left(-12+3r^6t^3 + 3r^4t(s-4t)-r^2(17s+30t)\right)\right),$$

$$d_{10} = dr^2s^2\left(r^2t-3\right)^2 + 16\pi\left(r^2t+1\right)^3 \left(r^2t\left(r^2\left(t\left(r^2t+3\right)+s\right)+3\right)+1\right),$$

$$d_{11} = 4096\pi^4 f^2r^2\left(r^2t+1\right)^{12}.$$

The transformation $x = r^2$ provides the expressions of the physical parameters $m_i(r)$, $u_i(r)$, $z_{g_i}(r)$ and $z_{s_i}(r)$ for intermediate layer ($R_c < r \le R_i$) as

$$m_i(r) = 4\pi\int r^2\rho_i dr = -\frac{r^3 s}{2\left(r^2t+1\right)^2}\,, \tag{34}$$

$$u_i(r) = \frac{m_i(r)}{r} - \frac{r^2 s}{2\left(r^2t+1\right)^2}\,, \tag{35}$$

$$z_{g_i}(r) = e^{-\nu_i/2} - 1\,, \tag{36}$$

$$z_{s_i}(r) = \frac{1}{\sqrt{1-2u_i(r)}} - 1\,. \tag{37}$$

3.3 Envelope-like Layer having Neutron Fluid or Coulomb Liquids and Quadratic EoS

For the envelope layer ($R_i \le r \le R_e$), we consider the same g_{rr} as above satisfying a quadratic EoS

$$z = e^{-\lambda_e} = 1 + \frac{sx}{(tx+1)^2}\,, \tag{38}$$

$$p_{r_e} = \alpha\rho^2 + \beta\rho - \gamma\,, \tag{39}$$

where s, t, α, β and γ are constants. Using Equations (7), (8), (10), (38) and (39), we obtain

$$\frac{y'(x)}{y(x)} + \frac{s+8\pi\gamma(tx+1)^2}{2\left(sx+(tx+1)^2\right)} = \frac{s(tx-3)\left(\alpha s(tx-3)+8\pi\beta(tx+1)^3\right)}{16\pi(tx+1)^4\left(sx+(tx+1)^2\right)}\,. \tag{40}$$

On integrating (40), we get

$$y_e = C_3\exp\left(\frac{\frac{d_{12}\tanh^{-1}(d_0)}{\sqrt{st^2}\sqrt{s+4t}} + d_{13} + d_{14}}{16\pi}\right), \tag{41}$$

where C_3 is an integration constant.

In view of Equations (38) and (41) and employing the transformation $x = r^2$, the field Equations (7)–(10) become

$$\rho_e = \frac{s\left(r^2t-3\right)}{8\pi\left(r^2t+1\right)^3}\,, \tag{42}$$

$$p_{r_e} = \frac{s\left(r^2t-3\right)\left(\alpha s\left(r^2t-3\right)+8\pi\beta\left(r^2t+1\right)^3\right)}{64\pi^2\left(r^2t+1\right)^6} - \gamma\,, \tag{43}$$

$$p_{t_e} = \frac{d_{15}+64\pi^2 s\left(r^2t+1\right)^6\left(d_{19}r^2s+d_{18}\right)+d_{20}}{2048\pi^3\left(r^2t+1\right)^{10}\left(r^2s+\left(r^2t+1\right)^2\right)}\,, \tag{44}$$

$$\Delta_e = p_{t_e} - p_{r_e}\,, \tag{45}$$

where

$$d_{12} = t^2\left(16\pi(\beta+1)s - \alpha\left(9s^2+42st+32t^2\right)\right) + 64\pi^2\gamma s(s+2t)\,,$$

$$d_{13} = \frac{\alpha\left(s(3tx(9tx+22)+55)+48t(tx+1)^2\right)}{3(tx+1)^3} - 64\pi^2\gamma x\,,$$

$$d_{14} = (\log(tx+1))^{(32\pi\beta-9\alpha s-24\alpha t)} + \left(\log\left(sx+(tx+1)^2\right)\right)^{\frac{\left(64\pi^2\gamma s+t^2(-32\pi\beta+9\alpha s+24\alpha t)\right)}{2t^2}}\,,$$

$$d_{15} = 16\pi\alpha d_{16}s^2\left(r^2t-3\right)\left(r^2t+1\right)^3 - 1024\pi^3\gamma d_{17}\left(r^2t+1\right)^9 + \alpha^2r^2s^4\left(r^2t-3\right)^4\,,$$

$$d_{16} = -6r^8t^4 + r^6t^2((\beta-6)s+24t) + 2r^4t((17-3\beta)s+30t) + 3r^2(3\beta s+8t) - 6\,,$$

$$d_{17} = 2r^6t^3 + r^4t((\beta+2)s+6t) + r^2(6t-3\beta s) + 2\,,$$

$$d_{18} = -4\beta\left(r^2t+1\right)^2\left(r^2t\left(r^2t-8\right)+3\right),$$

$$d_{19} = -18\alpha\gamma + 9\beta^2 + r^4t^2(-2\alpha\gamma+(\beta-4)\beta-1) + 2r^2t(6\alpha\gamma+\beta(14-3\beta)+1)+3\,,$$

$$d_{20} = 4096\pi^4\gamma^2r^2\left(r^2t+1\right)^{12}\,.$$

The parameters $m_e(r)$, $u_e(r)$, $z_{g_e}(r)$ and $z_{s_e}(r)$ for the envelope layer ($R_i < r \le R_e$) when $x = r^2$ are as

follows

$$m_e(r) = 4\pi \int r^2 \rho_e dr = -\frac{r^3 s}{2\left(r^2 t+1\right)^2}, \quad (46)$$

$$u_e(r) = \frac{m_e(r)}{r} = -\frac{r^2 s}{2\left(r^2 t+1\right)^2}, \quad (47)$$

$$z_e(r) = e^{-\nu_e/2} - 1, \quad (48)$$

$$z_{s_e}(r) = \frac{1}{\sqrt{1-2u_e(r)}} - 1. \quad (49)$$

4 MATCHING AT THE JUNCTIONS OF LAYERS AND BOUNDARY

For well-behaved solutions, all the three interfaces, i.e, core-intermediate (C-I), intermediate-envelope (I-E) and envelop-boundary (E-B) interfaces, are required to match for continuity of the physical parameters considering Dormois-Israel conditions.

4.1 Continuity of C-I layer junction

The core layer metric (11) should be matched smoothly with intermediate layer metric (12) at $r = R_c$, that is,

$$e^{\lambda_c}(R_c) = e^{\lambda_i}(R_c), \quad (50)$$

$$e^{\nu_c}(R_c) = e^{\nu_i}(R_c), \quad (51)$$

and ρ_r must be continuous at $r = R_c$, i.e.,

$$p_{r_c}(R_c) = p_{r_i}(R_c). \quad (52)$$

It implies that

$$a\rho(R_c) - b = \nu\rho^2(R_c) - \delta.$$

4.2 Continuity of I-E Layer Junction

The intermediate layer metric (12) must be matched smoothly with envelope layer metric (13) at $r = R_i$, that is,

$$e^{\lambda_i}(R_i) = e^{\lambda_e}(R_i), \quad (53)$$

$$e^{\nu_i}(R_i) = e^{\nu_e}(R_i), \quad (54)$$

and ρ_r must be continuous at $r = R_i$, that is,

$$p_{r_i}(R_i) = p_{r_e}(R_i). \quad (55)$$

It implies that

$$\nu\rho^2(R_c) - \delta = \alpha\rho^2(R_i) + \beta\rho(R_i) - \gamma.$$

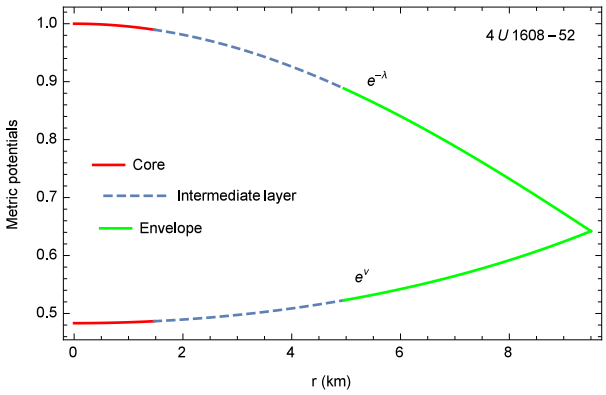

Fig. 2 Variation in metric potentials with r for the X-ray binary star 4U 1608–52.

4.3 Continuity of E-B Interface

The envelope metric (13) must be connected smoothly over the boundary with the Schwarzschild exterior solution

$$ds^2|_b = \left(1-\frac{2M}{r}\right)dt^2 - \left(1-\frac{2M}{r}\right)^{-1}dr^2 - r^2(d\theta^2 + \sin^2\theta d\phi^2)$$

at the pressure free boundary Σ (defined by $r = R_e$). Continuities of e^{λ} and e^{ν} across the boundary are known as the first fundamental form of the Dormois-Israel junction condition $[ds^2]_\Sigma = 0$, yielding

$$e^{\lambda_e}(R_e) = \left(1-\frac{2M}{R_e}\right)^{-1}, \quad (56)$$

$$e^{\nu_e}(R_e) = \left(1-\frac{2M}{R_e}\right). \quad (57)$$

On the other hand, ρ_r should vanish at the surface of the star ($r = R_e$), i.e.,

$$p_{r_e}(R_e) = 0. \quad (58)$$

The above expression corresponds to the second fundamental form $[G_{\mu\nu}x^\nu]_\Sigma = 0$, where x^ν denotes unit vector projected in the radial direction.

Using Equation (58), we have

$$\alpha\rho^2(R_e) + \beta\rho(R_e) - \gamma = 0,$$

where R_e is the radius of the star.

The nine interface conditions (50)–(58) along with the sixteen constants, namely s, t, a, b, d, f, α, β, γ, C_1, C_2, C_3, R_c, R_i, R_e and M, form an undetermined system of equations. Solving the above system of equations, mass M, core radius R_c, intermediate radius R_i and envelope radius R_e of the star can be obtained from the following expressions:

$$M = -\frac{R_e^3 s}{2\left(R_e^2 t+1\right)^2}, \quad (59)$$

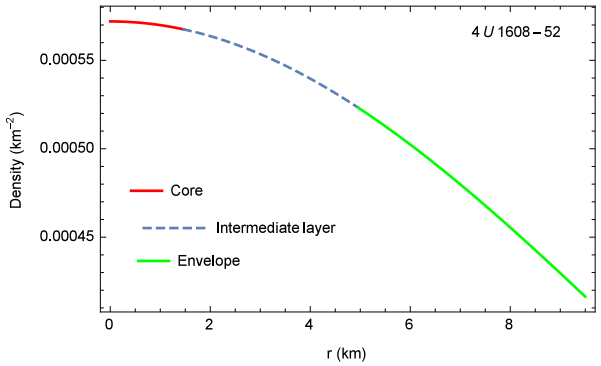

Fig. 3 Variation of density with r for the X-ray binary star 4U 1608–52.

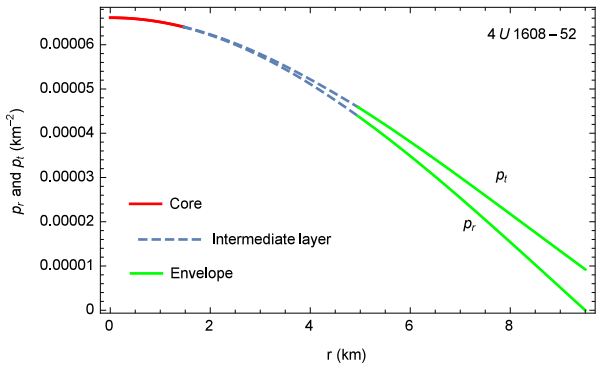

Fig. 4 Variation of radial and tangential pressures with r for the X-ray binary star 4U 1608–52.

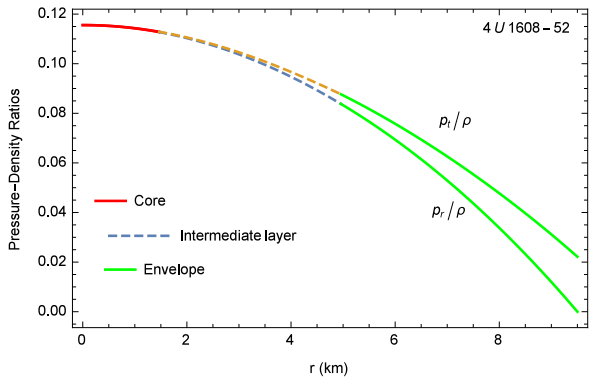

Fig. 5 Variation of pressure density ratios (p_r/ρ, p_t/ρ) with r for the X-ray binary star 4U 1608–52.

$$b = \frac{s\left(\frac{\left(R_e^2t-3\right)\left(\alpha s\left(R_e^2t-3\right)+8\pi\beta\left(R_e^2t+1\right)^3\right)}{\left(R_e^2t+1\right)^6}+\sigma_1-\sigma_2\right)}{64\pi^2}, \tag{60}$$

$$f = \frac{s\left(\frac{\alpha s}{\left(R_e^2t+1\right)^4}+\frac{8\pi\beta}{\left(R_e^2t+1\right)^2}-\frac{32\pi\beta}{\left(R_e^2t+1\right)^3}+\sigma_3+\sigma_4\right)}{64\pi^2}, \tag{61}$$

$$\gamma = \frac{s\sigma_5\left(R_e^2t-3\right)}{64\pi^2\left(R_e^2t+1\right)^6}, \tag{62}$$

and the remaining constants $C_3,\ C_2$ and C_1 are evaluated as

$$C_3 = \frac{\left(R_e-2M\right)\tau_1\exp\left(-\frac{\frac{\tau_3\tanh^{-1}(\sigma_e)}{\sqrt{s}t^2\sqrt{s+4t}}+\tau_2}{48\pi}\right)}{R_e}, \tag{63}$$

$$C_2 = \tau_4C_3\left(R_i^2t+1\right)^{2\beta+\frac{3(d-\alpha)(3s+8t)}{16\pi}} \times\exp\left(-\frac{\frac{3\tau_5\tanh^{-1}(\sigma_i)}{\sqrt{s}t^2\sqrt{s+4t}}+\tau_6}{48\pi}\right), \tag{64}$$

$$C_1 = \tau_7C_2\left(R_c^2t+1\right)^{-2a-\frac{3d(3s+8t)}{16\pi}} \times\exp\left(-\frac{\frac{3\tau_9\tanh^{-1}(\sigma_c)}{\sqrt{s}t^2\sqrt{s+4t}}+\tau_8}{48\pi}\right), \tag{65}$$

where

$$\sigma_k = \frac{2t\left(R_k^2t+1\right)+s}{\sqrt{s}\sqrt{s+4t}} \quad \text{for } k=e,\ i,\ c,$$

$$\sigma_1 = \frac{8\pi a\left(R_c^2t-3\right)}{\left(R_c^2t+1\right)^3}-\frac{ds\left(R_c^2t-3\right)^2}{\left(R_c^2t+1\right)^6} +\frac{ds\left(R_i^2t-3\right)^2}{\left(R_i^2t+1\right)^6},$$

$$\sigma_2 = \frac{\left(R_i^2t-3\right)\left(\alpha s\left(R_i^2t-3\right)+8\pi\beta\left(R_i^2t+1\right)^3\right)}{\left(R_i^2t+1\right)^6},$$

$$\sigma_3 = \frac{2R_i^2t(32\pi\beta-3ds+3\alpha s)}{\left(R_i^2t+1\right)^6}+\frac{16\alpha s}{\left(R_e^2t+1\right)^6} -\frac{8\pi\beta R_i^8t^4}{\left(R_i^2t+1\right)^6},$$

$$\sigma_4 = \frac{24\pi\beta+R_i^4t^2(48\pi\beta+ds-\alpha s)+9ds-9\alpha s}{\left(R_i^2t+1\right)^6} -\frac{8\alpha s}{\left(R_e^2t+1\right)^5},$$

$$\sigma_5 = 8\pi\beta+R_e^2t\left(24\pi\beta+8\pi\beta R_e^2t\left(R_e^2t+3\right)+\alpha s\right) -3\alpha s,$$

$$\tau_1 = \left(R_e^2s+\left(R_e^2t+1\right)^2\right)^{\beta-\frac{2\pi\gamma s}{t^2}-\frac{3\alpha(3s+8t)}{32\pi}} \times\left(R_e^2t+1\right)^{\frac{3\alpha(3s+8t)}{16\pi}-2\beta},$$

$$\tau_2 = \frac{\alpha\left(s\left(3R_e^2t\left(9R_e^2t+22\right)+55\right)+48t\left(R_e^2t+1\right)^2\right)}{\left(R_e^2t+1\right)^3} -192\pi^2\gamma R_e^2,$$

$$\tau_3 = 3\left(t^2\left(16\pi(\beta+1)s-\alpha\left(9s^2+42st+32t^2\right)\right)\right) +192\pi^2\gamma s(s+2t),$$

$$\tau_4 = \left(R_i^2(s+2t)+R_i^4t^2+1\right)^{-\beta-\frac{3(d-\alpha)(3s+8t)}{32\pi}-\frac{2\pi fs}{t^2}+\frac{2\pi\gamma s}{t^2}},$$

$$\tau_5 = t^2\left((d-\alpha)\left(-\left(9s^2+42st+32t^2\right)\right)-16\pi\beta s\right) +64\pi^2fs(s+2t)-64\pi^2\gamma s(s+2t),$$

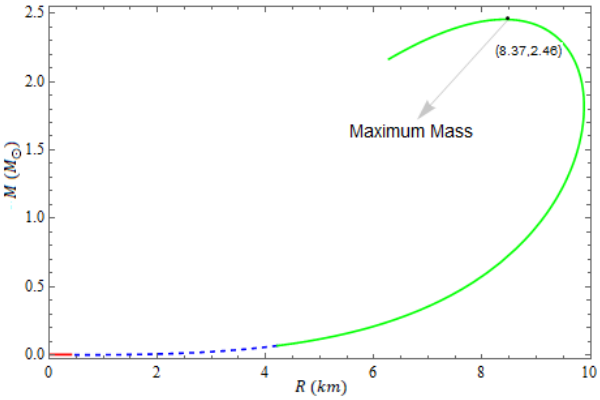

Fig. 6 Variation of mass with R.

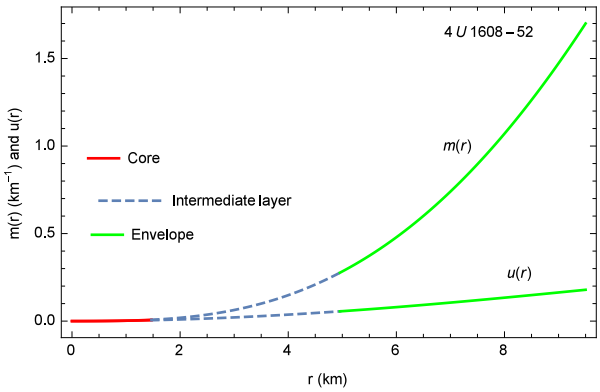

Fig. 7 Variation of mass and compactification factor with r for the X-ray binary star 4U 1608–52.

$$\tau_6 = 3R_i^2\left(\frac{t(d-\alpha)\left(R_i^2t(9s+16t)+22s+32t\right)}{(R_i^2t+1)^3}\right) + 192R_i^2\pi^2(\gamma-f)+\frac{(d-\alpha)(55s+48t)}{(R_i^2t+1)^3},$$

$$\tau_7 = \left(R_c^2s+\left(R_c^2t+1\right)^2\right)^{a+\frac{2\pi s(f-b)}{t^2}+\frac{3d(3s+8t)}{32\pi}},$$

$$\tau_8 = 192\pi^2R_c^2(f-b)+ \frac{d\left(-3R_c^2t\left(R_c^2t(9s+16t)+22s+32t\right)-55s-48t\right)}{(R_c^2t+1)^3},$$

$$\tau_9 = t^2\left(16\pi as+9ds^2+42dst+32dt^2\right) + 64\pi^2bs(s+2t)-64\pi^2fs(s+2t).$$

The constants s, t, a, b, d, f, α, β and γ are free parameters.

5 INVESTIGATION OF WELL-BEHAVED STELLAR MODEL

5.1 Geometrical Regularity

The metric potentials $e^{-\lambda}$ and e^{ν} of the star 4U 1608–52 at the center of the core $r = 0$ are finite, positive, non-singular and $e^{\lambda}|_{r=0} = 1$. Further, both $e^{-\lambda}$ and e^{ν} are monotonically increasing and decreasing outward respectively besides being continuous at all the three interfaces (Fig. 2).

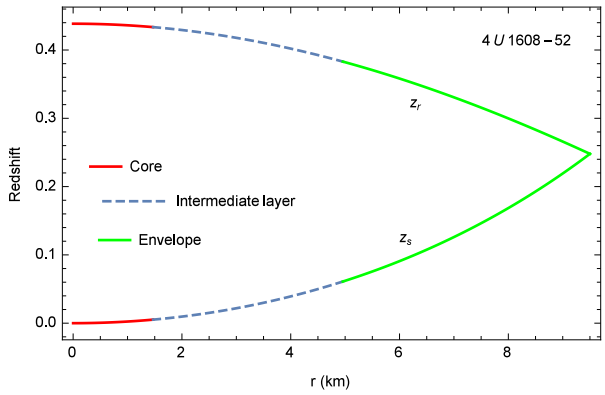

Fig. 8 Variation of gravitational and surface redshifts $(z_i(r),\ z_s(r))$ with r for the X-ray binary star 4U 1608–52.

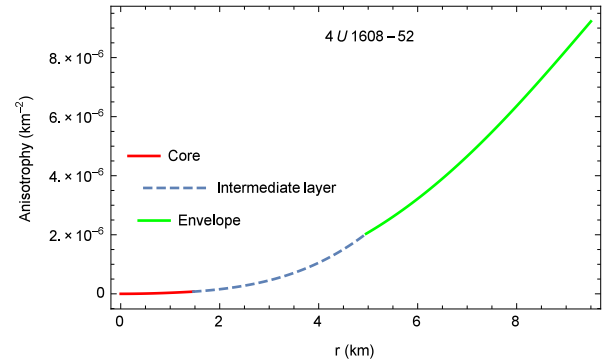

Fig. 9 Variation of anisotropy $(\Delta(r))$ with r for the X-ray binary star 4U 1608–52.

5.2 Trends of Physical Parameters

5.2.1 Density and pressures

The matter density ρ and pressures p_r and p_t for all the three layers of the X-ray binary star 4U 1608–52 are positive and monotonically decreasing outward (Figs. 3 and 4) besides being continuous at the respective interfaces. The non-singularity and positiveness of p_r, p_t and ρ at the center provide a regular solution, i.e.,

$$p_{r0} = p_{t0} = -\frac{3as}{8\pi} - b > 0\,, \tag{66}$$

$$\rho_0 = -\frac{3s}{8\pi} > 0 \text{ for } s < 0\,. \tag{67}$$

Regularity of any physical solution is verified by the Zeldovich criterion, i.e., $\frac{p_{r0}}{\rho_0} \leq 1$ (Zeldovich 1962)

$$\frac{p_{r0}}{\rho_0} = a + \frac{8\pi b}{3s} < 1\,. \tag{68}$$

On solving Equations (66), (67) and (68), we obtain the following inequality

$$\frac{3(1-a)s}{8\pi} < b < \frac{-3as}{8\pi}\,. \tag{69}$$

p_r/ρ and p_t/ρ are positive and less than 1 throughout the inside of the star and are continuous at the junctions (Fig. 5).

5.2.2 *Mass-radius, compactification and redshift:*

Mass ($m(r)$), compactification factor ($u(r)$) and gravitational and surface redshifts ($z_g(r),\ z_s(r)$) for all the three layers of the X-ray binary star 4U 1608–52 are continuous at the interfaces. The increasing nature of the parameters $m(r)$ and $u(r)$, and $z_s(r)$ and decreasing trend of $z_g(r)$ with radial coordinate r are plotted in Figures 7 and 8, respectively. Also, from Figure 7, it is clearly visible that $u(r)$ for the star 4U 1608–52 lies within the Buchdahl limit (Buchdahl 1959) from the center to surface of the star. From Figure 6, one can observe that the maximum mass $2.46\ M_\theta$ is obtained for radius 8.37 km, which is within the proposed limit of Rhoades & Ruffini (1974).

5.2.3 *Anisotropy*

In Figure 9, the radial pressure coincides with the tangential pressure at the core of the star, is continuous at all the interfaces and increasing outward (Herrera & Santos 1997).

5.2.4 *Causality condition*

The radial and tangential sound speeds ($v_r^2,\ v_t^2$) of a compact star model satisfy the causality condition throughout the interior of the star ($0 < v_r^2,\ v_t^2 < 1$). Figure 10 demonstrates that v_r^2 and v_t^2 are decreasing functions of r throughout the interior of 4U 1608–52 but the continuity of the graph at the interfaces is obtained for v_r^2 but not for v_t^2. For the star SAX J1808.4–3658, both the sound speeds ($v_r^2,\ v_t^2$) are monotonically decreasing outward besides being continuous at all the respective interfaces (Fig. 11).

5.2.5 *Adiabatic index*

For a relativistic anisotropic sphere, stability depends on the adiabatic index Γ_r. Corresponding to three layers, Γ_{r_l} is defined as (Heintzmann & Hillebrandt 1975),

$$\Gamma_{r_l} = \frac{\rho+p_{r_l}}{p_{r_l}} v_{r_l}^2,$$

for $l = c, i$ and e. The trend of adiabatic index for all the three layers of the binary star 4U 1608–52 is plotted in Figure 12, where the adiabatic index is continuous

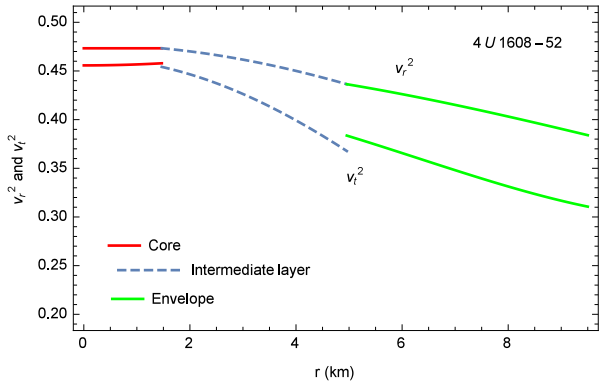

Fig. 10 Variation of radial and transverse sound speeds with r for the X-ray binary star 4U 1608–52.

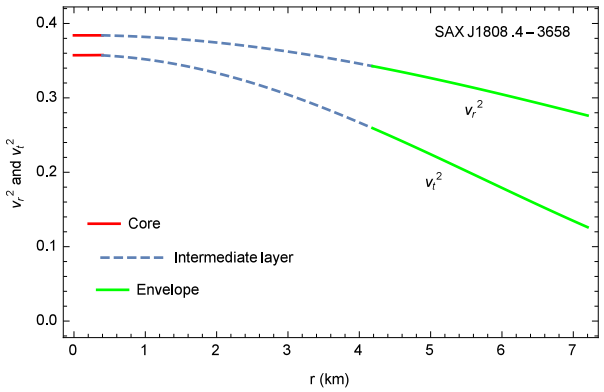

Fig. 11 Variation of radial and transverse sound speeds with r for the star SAX J1808.4–3658.

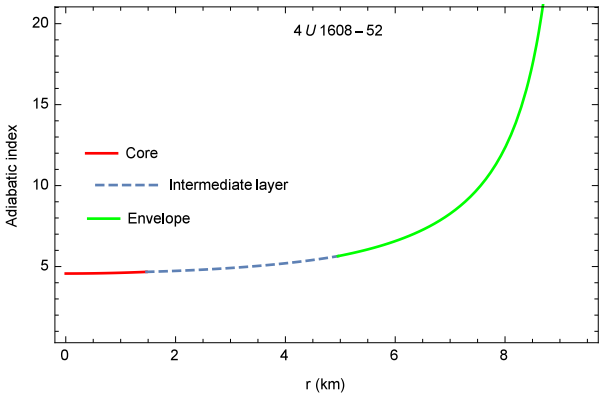

Fig. 12 Variation of adiabatic index (Γ) with r for the X-ray binary star 4U 1608–52.

at all the interfaces and satisfies the condition $\Gamma_{r_l} > \frac{4}{3}$. In the interior of stellar objects, $\Gamma_r \geq \Gamma_{\rm critical} = \frac{4}{3} + \frac{19}{42}(2U_R)$. It is important to note that this relation is only valid for nearly Newtonian stars with uniform densities (Chandrasekhar 1964a,b; Moustakidis 2017). Here, $\Gamma_{\rm critical}$ depends linearly on the pressure-density ratio at the center and can be evaluated as

Table 1 Values of Free Parameters ($s,\ t,\ a,\ b,\ d,\ f,\ \alpha,\ \beta,\ \gamma$ in $(\text{km})^{-2}$) to Obtain Mass, Radi of Core, Inner and Envelope Layers (R_c, R_i and R_e in km) for the Binary Star 4U 1608–52.

s	t	a	b	d	f	α	β	γ
-0.48×10^{-2}	1.1×10^{-3}	0.47	2.05×10^{-4}	417	7.03×10^{-5}	245	0.18	1.17×10^{-4}
R_c	R_i	R_e	M					
1.47	4.9576	9.5	$1.7\,M_\odot$					

Table 2 Values of Free Parameters ($s,\ t,\ a,\ b,\ d,\ f,\ \alpha,\ \beta,\ \gamma$ in $(\text{km})^{-2}$) to Obtain Mass, Radi of Core, Inner and Envelope Layers (R_c, R_i and R_e in km) for the Star SAX J1808.4–3658.

s	t	a	b	d	f	α	β	γ
-0.78×10^{-2}	2×10^{-3}	0.38	2.7×10^{-4}	205.6	9.26×10^{-5}	205	0.001	9.31×10^{-5}
R_c	R_i	R_e	M					
0.399918	4.18522	7.2	$1.2\ M_\odot$					

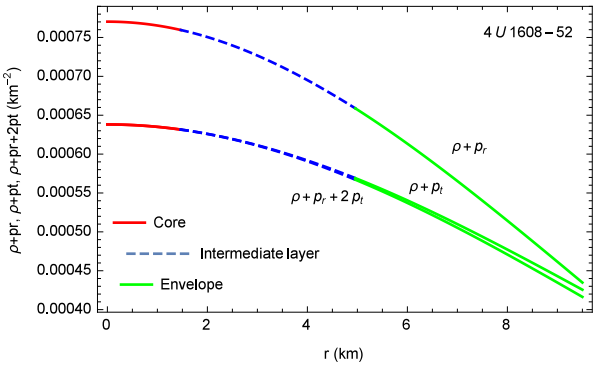

Fig. 13 Variation of energy conditions with r for the X-ray binary star 4U 1608–52.

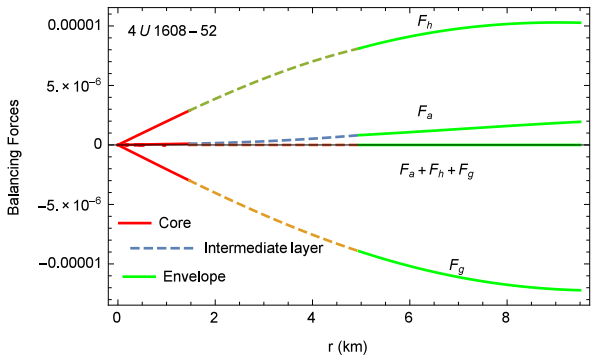

Fig. 14 Variation of balancing forces with r for the X-ray binary star 4U 1608–52.

$$\frac{p_{r0}}{\rho_0} = \frac{3a\left(R_e^2t+1\right)^2U_R - 4\pi bR_e^2}{3(R_e^2t+1)^2U_R},$$

where $U_R = \frac{M}{R_e}$. In this model $\Gamma_r \geq \Gamma_{\text{critical}} = 1.4952380952$ for 4U 1608–52 and $\Gamma_r \geq \Gamma_{\text{critical}} = 1.48412698$ for SAX J1808.4–3658.

5.2.6 *Energy conditions*

For a physically stable configuration, all the three layers of the star should satisfy the three energy conditions (Maurya et al. 2019): (i) Null energy condition $\rho + p_r \geq 0$ (NEC) (ii) Weak energy conditions $\rho + p_r \geq 0$, $\rho \geq 0$ (WEC_r) and $\rho + p_t \geq 0$, $\rho \geq 0$ (WEC_t) and (iii) Strong energy condition $\rho + p_r + 2p_t \geq 0$ (SEC). The variations of energy conditions with r for the star 4U 1608–52 in all the three layers are continuous at the interfaces and satisfy realistic conditions as seen in Figure 13.

5.2.7 *Static stability criterion using modified TOV equation*

In the equilibrium state, the resulting gravitational (F_g), hydrostatic (F_h) and anisotropic (F_a) forces should be zero throughout the interior of the star and continuous at the interfaces. The Tolman-Oppenheimer-Volkoff (TOV) equation (Ponce de Leon 1987) for the respective three layers ($l = c,\ i,\ e$) is given as

$$-\frac{\nu_l'(\rho + p_{r_l})}{2} - \frac{dp_{r_l}}{dr} + \frac{2\Delta_l(r)}{r} = 0\,. \tag{70}$$

From Figure 14, we can ascertain that the TOV condition is satisfied within the star 4U 1608–52 and all the three forces are continuous at all the interfaces, thereby, concluding that the system is in static equilibrium.

5.2.8 *Herrera cracking stability criterion*

For the values mentioned in Tables 1 and 2, the Herrera cracking condition, i.e., $-1 < v_t^2 - v_r^2 < 0$ is attained for both the compact stars 4U 1608–52 and SAX J1808.4–3658. The continuity of the profile of $v_t^2 - v_r^2$ is obtained for the star SAX J1808.4–3658, but not for the binary star 4U 1608–52 due to the continuity and discontinuity of the graphs of v_t at the interfaces of the star respectively (Figs. 15 and 16).

6 DISCUSSION AND CONCLUSION OF THREE LAYERED HYBRID MODEL

In the present article, we have studied a three layered anisotropic stellar model, where the core part is outfitted

with the MIT bag EoS, inner part equipped with modified BEC EoS and envelope part augmented with quadratic EoS to interpret the interior structure of stellar objects.

The three layered model is viable in all aspects for the X-ray binary (low-mass X-ray binary, LMXB) star 4U 1608–52 and the potentially strange star SAX J1808.4–3658. We have analyzed the model entirely for the star 4U 1608–52 through graphical representations of suitable parameter values (see Tables 1 and 2).

The geometrical and physical attributes like $e^{-\lambda}$, $p_r(r)$, $p_t(r)$, $\rho(r)$, p_r/ρ, p_t/ρ, $z_g(r)$, $z_s(r)$, v_r^2 and v_t^2 and all the energy conditions for the binary star 4U 1608–52 are non-negative at the center and satisfy the Zeldovich condition throughout interior of the star 4U 1608–52. Decreasing trends of these physical attributes from the center to the surface of the star are displayed in Figures 2, 4, 3, 5, 8, 10 and 13. Increasing trends of other physical and geometrical attributes, i.e., e^{ν}, $m(r)$, $u(r)$, $\Delta(r)$ and $\Gamma(r)$ from center to surface of the star are exhibited in Figures 2, 7, 9 and 12. Our three layer model fulfills all stable criteria mentioned in Pant et al. (2020) in all the three regions for the star 4U 1608–52, i.e.,

(i) the adiabatic index $\Gamma(r) \geq \frac{4}{3}$, (Fig. 12) which concludes that our model fulfills the Bondi adiabatic condition (Bondi 1964).

(ii) the difference in sound speeds $v_t^2 - v_r^2$ lies in the interval $(-1, 0)$ (see Fig. 15), which demonstrates that the hybrid model is potentially stable. However, the tangential sound speed v_t^2 and the stability factor $v_t^2 - v_r^2$ are not continuous (removable discontinuity) at the interfaces of star 4U 1608–52.

(iii) the model represents a stable, static equilibrium configuration in all the three regions by satisfying the generalized TOV-equation (Fig. 14).

Further, we have ascertained that the parameters, namely, $e^{\lambda(r)}$, $e^{\nu(r)}$, $p_r(r)$, $p_t(r)$, $\rho(r)$, p_r/ρ, p_t/ρ, $\Delta(r)$, $m(r)$, $u(r)$, $z_g(r)$, $z_s(r)$, energy conditions, $\Gamma(r)$, $v_r^2(r)$ and TOV equation of forces are continuous and well behaved from the center to the surface of the star SAX J1808.4–3658. In Glendenning (2000), it has been observed that energy jumps are perfectly consistent with stable stars which is a common consequence of first-order phase transitions. Due to low mass of SAX J1808.4–3658, the graphical representations of v_t^2 and the stability factor $v_t^2 - v_r^2$ may lead to continuity at the interfaces (Figs. 11 and 16).

The magnitudes of the physical attributes $\Gamma(r)$, $\rho(r)$, $p_r(r)$ and $z_g(r)$ at the center, interfaces and boundary for the stars 4U 1608–52 and SAX J1808.4–3658 are expressed in Tables 3 and 4 for the parameter values displayed in Tables 1 and 2. From the tables, we notice that the values of the physical quantities $\Gamma(r)$, $\rho(r)$ and

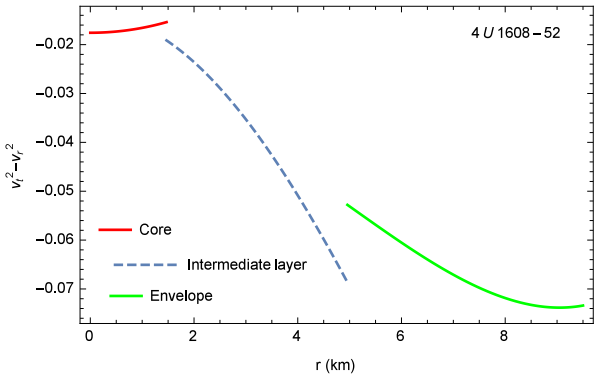

Fig. 15 Variation of stability factor with r for the X-ray binary star 4U 1608–52.

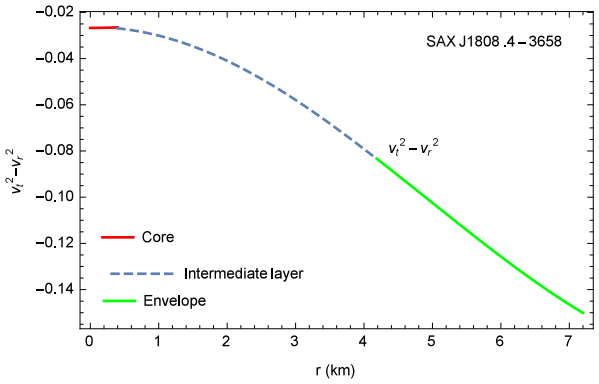

Fig. 16 Variation of stability factor with r for the star SAX J1808.4–3658.

$z_g(r)$ at the center and core-intermediate interface increase with higher mass of the stars whereas radial pressure at the center and core-intermediate interface decreases with higher mass of the stars. At the boundary, with increase in the mass of the stars, the parameters like density and surface redshift also increase and $z_g(r)$ and $z_s(r)$ coincide at the boundary of the star whereas parameters like adiabatic index and radial pressure decrease. It may be observed that continuity of the stability factor in all the three regions of the star demands a smaller core. As the core region of the stars increases, the stability factor becomes discontinuous at all interfaces of the regions.

7 GENERATING FUNCTIONS OF THREE LAYERS

The primitive generating functions related to the geometry of space-time ($\zeta(r)$) and matter distribution ($\Pi(r)$) for spherically symmetric anisotropic systems are described as (Herrera et al. 2008)

$$\begin{aligned} e^{\nu(r)} &= e^{\left[\int (2\zeta(r) - \frac{2}{r})dr\right]}, \\ \Pi(r) &= 8\pi(p_r - p_t). \end{aligned} \tag{71}$$

Table 3 Variations in $\Gamma(r)$, $\rho(r)$, $p_r(r)$ and $z_g(r)$ of the Star 4U 1608–52 and $G = 0.667 \times 10^{-10}\,\mathrm{m^3\,kg^{-1}\,s^{-2}}$, $M_\odot = 2 \times 10^{30}\,\mathrm{kg}$ and $C = 3 \times 10^8\,\mathrm{m\,s^{-1}}$.

	Center	Core-inner layer junction	Inner layer-envelope junction	Surface
$\Gamma(r)$	4.5686	4.6718	5.6439	∞
$\rho(r)$ ($\mathrm{g\,cm^{-3}} \times 10^{14}$)	2.8878	2.8833	2.8366	2.7
$p_r(r)$ ($\mathrm{dyne\,cm^{-2}} \times 10^{35}$)	3.192	3.0893	1.4612	0
$z_g(r)$	0.4385	0.4335	0.383	0.2117

Table 4 Variations in $\Gamma(r)$, $\rho(r)$, $p_r(r)$ and $z_g(r)$ of the Star SAX J1808.4 – 3658 and $G = 0.667 \times 10^{-10}\,\mathrm{m^3\,kg^{-1}\,s^{-2}}$, $M_\odot = 2 \times 10^{30}\,\mathrm{kg}$ and $C = 3 \times 10^8\,\mathrm{m\,s^{-1}}$.

	Center	Core-inner layer junction	Inner layer-envelope junction	Surface
$\Gamma(r)$	4.5085	4.5223	6.0406	∞
$\rho(r)$ ($\mathrm{g\,cm^{-3}} \times 10^{14}$)	2.876	2.875	2.816	2.7
$p_r(r)$ ($\mathrm{dyne\,cm^{-2}} \times 10^{35}$)	4.204	4.185	2.42	0
$z_g(r)$	0.3903	0.3898	0.3312	0.2247

The two generating functions $\zeta(r)$ and $\Pi(r)$ of our model in each layer for the X-ray binary star 4U 1608-52 are obtained as

$$\zeta_c = \frac{r^2\left(r^2t\left((a+1)s+2t\left(r^2t+3\right)\right)+\Phi_1\right)+2}{2r\left(r^2t+1\right)\left(r^2\left(t\left(r^2t+2\right)+s\right)+1\right)},$$

$$\zeta_i = \frac{8\pi\left(r^2t+1\right)^4\left(r^2\left(2t\left(r^2t+2\right)+s\right)+2\right)+\varphi_2}{16\pi r\left(r^2t+1\right)^4\left(r^2\left(t\left(r^2t+2\right)+s\right)+1\right)},$$

$$\zeta_e = \frac{8\pi\phi_4\left(r^2t+1\right)^3+\Phi_3}{16\pi r\left(r^2t+1\right)^4\left(r^2\left(t\left(r^2t+2\right)+s\right)+1\right)},$$

and

$$\Pi_l(r) = 8\pi(p_{r_l} - p_{t_l}) \text{ for } l = c,\ i \text{ and } e,$$

$$\phi_1 = -3as - 8\pi b\left(r^2t+1\right)^3 + s + 6t\,,$$

$$\phi_2 = dr^2s^2\left(r^2t-3\right)^2 - 64\pi^2 f r^2\left(r^2t+1\right)^6,$$

$$\phi_3 = \alpha r^2s^2\left(r^2t-3\right)^2 - 64\pi^2\gamma r^2\left(r^2t+1\right)^6\,,$$

$$\phi_4 = 2r^6t^3 + r^4t(\beta s + s + 6t) + r^2(-3\beta s + s + 6t) + 2\,.$$

Acknowledgements The authors are thankful to the learned referees for their valuable suggestions that improved the paper.

References

Abreu, H., et al. 2007, CQG, 24, 4631

Abuki, H. 2007, Nucl. Phys. A, 791, 117

Alford, M. 2001, Annu. Rev. Nucl. Part. Sci., 51, 131

Banik, S., & Bandyopadhyay, D. 2003, Phys. Rev. D, 67,123003

Banik, S., et al. 2004, Phys. Rev. D, 70, 123004

Baym, G., & Pethick, C. 1979, Annual Review of Astronomy and Astrophysics, 17, 415

Bedaque, P. F., & Schafer, T. 2002, Nucl. Phys. A, 697, 802

Bhar, P., Murad, M. H., & Pant, N. 2015, Astrophys. Space Sci., 359, 13

Bhar, P., Singh, K. N., & Pant, N. 2016, Ap&SS, 361, 343

Bhar, P., Singh, K. N., & Pant, N. 2017, Indian Journal of Physics, 91, 701

Bhar, P., Govender, M., & Sharma, R. 2018, Pramana-J. Phys., 90, 5

Benaoum, H. B. 2002, arXiv:hep-th/0205140

Bondi, H. 1964, Proc. R. Soc. Lond. A, 281, 39

Buchdahl, H.A. 1959, Physical Review, 116, 1027

Chan, R., Silva, M. F. A. D., & Rocha, P. 2011, Gen. Relativ. Gravit., 43, 2223

Chandrasekhar, S. 1964, Astrophys, J., 140, 417

Chandrasekhar, S. 1964, PRL, 12, 114

Chavanis, P. H., & Harko, T. 2012, Phys. Rev. D, 86, 064011

Cheng, K. S, Dai, Z. G., & Lu, T. 1998, Int. J. Mod. Phys. D, 7, 139

Colpi, M., Shapiro, S. L., & Wasserman, I. 1986, Phys. Rev. Lett., 57, 2485

Das, P. K., & Narlikar, J. V. 1975, Monthly Notices Roy. Astron. Soc., 171, 87

Drago, A., & Lavagno, A. 2001, Phys. Lett. B, 511, 229

Durgapal, M.C., & Gehlot, G. L. 1969, Phys. Rev. D, 183, 1102

Durgapal, M.C., & Gehlot, G. L. 1971, J. Phys. A, 4, 749

Esculpi, M., & Alomá, E. 2010, Eur. Phys. J. C, 67, 521

Farhi, E., & Jaffe, R. L. 1984, Phys. Rev. D, 30, 2379

Feroze, T., & Siddiqui, A. A. 2011, Gen. Relativ. Gravit., 43, 1025

Gangopadhyay, T., et al. 2013, Mon. Not. R. Astron. Soc., 431, 3216

Gedela, S., et al. 2019, Eur. Phys. J. C, 79, 566

Gedela, S., Pant, N., Pant, R. P, & Upreti, J. 2019, Int. J. Mod. Phys. A., 34, 1950179

Ginzburg, V. L. 1969, Usp. Fiz. Nauk, 97, 601

Ginzberg, V. L. 1971, Usp. Fiz. Nauk, 103, 393

Glendenning, N. K. 1992, Phys. Rev. D, 46, 1274

Glendenning, N.K. 2000, Compact Stars: Nuclear Physics,Particle Physics and General Relativity(2nd ed.), New York, Springer
Govender, M., Bogadi, R. S., & Maharaj, S. D. 2017, Int. J. Mod. Phys. D, 26, 1750065
Govender, M., Mewalal, N., & Hansraj, S. 2019, Eur. Phys. J. C, 79, 24
Hansraj, S., Maharaj, S. D., & Mlaba, S. 2016, Eur. Phys. J. Plus, 131, 4
Heintzmann, H., & Hillebrandt, W. 1975, Astron. Astrophys., 38, 51
Heiselberg. H 2001, Int. J. Mod. Phys., 15, 1519
Heiselberg. H., & Hjorth-Jensen. M. 2000, Phys. Rept., 328, 237
Herrera, L. 1992, Physics Letters A, 165, 206
Herrera, L., et al. 2008, Phys. Rev. D, 77, 027502
Herrera, L., & Santos, N. O. 1997, Phys. Rep., 286, 53
Herrera, L. 2020, Phys. Rev. D, 101, 104024
Kapusta, J. I. 2004, Phys. Rev. Lett., 93, 251801
Kettner, Ch., Weber, F., Weigel, M. K., & Glendenning, N. K. 1995, Phys. Rev. D, 51, 1440
Lattimer, J. M., & Prakash, M 2004, Science, 304, 536
Maharaj, S. D., & Takisa, P. M. 2012, Gen. Relativ. Gravit., 44, 1419
Mann, A. 2020, Nature, 579, 20
Maurya, S. K., et al. 2019, Phys. Rev. D, 99, 044029
Migdal, A. B. 1960, Sov. Phys. JETP, 10, 176
Moustakidis, Ch. C. 2017, Gen. Relativ. Gravit., 49, 68
Ngubelanga, S. A., & Maharaj, S. D. 2017, Astrophys. Space Sci., 362, 43
Noureen, I., et al. 2019, Eur. Phys. J. C, 79, 302
Pant, N., Gedela, S., et al. 2020, European Physical Journal Plus, 135, 180
Pant, R. P., et al. 2019, Eur. Phys. J. C, 79, 602
Paul, B. C., & Tikekar, R. 2005, Gravit. Cosmol., 11, 244
Phukon, T. C. 2000, Phys. Rev. D, 62, 023002
Pisalski, R. D., & Wilczek, F. 1984, Phys. Rev. Lett., 29, 338
Ponce de Leon, J. 1987, Gen. Relativ. Gravit., 19, 797
Potekhin, A. Y. 2010, Phys.-Usp., 53, 1235
Rahaman.F., et al. 2010, Phys.Rev. D, 82, 104055
Rahaman, F., et al. 2012, Phys. Lett. B, 707, 319
Rahaman, F., et al. 2012, Phys. Lett. B, 717, 1
Rhoades, C. E. Jr., & Ruffini, R. 1974, Phys. Rev. Lett., 32, 324.
Ruderman, M. 1968, Nature, 218, 1128
Sharma, R., & Maharaj, S. D. 2007, Mon. Not. R. Astron. Soc., 375, 1265
Sharma, R., & Mukherjee, S. 2001, Mod. Phys. Lett. A, 16, 1049
Sharma, R., & Mukherjee, S. 2002, Mod. Phys. Lett. A, 17, 2535
Singh, K. N., et al. 2020, Physics of the Dark Universe, 29, 100575
Singh, K. N., et al. 2020, Physics of the Dark Universe, 30, 100620
Sunzu, J. M., & Thomas, M. 2018, Pramana C J. Phys., 91, 75
Takisa, P. M., & Maharaj, S. D. 2013, Astrophys. Space Sci., 343, 569
Takisa, P.M., & Maharaj, S. D. 2013, Gen. Rel. Grav., 45, 1951
Takisa, P. M., & Maharaj, S.D. 2016, Astrophys. Space Sci., 361, 262
Takisa, P. M., Ray, S., & Maharaj, S. D. 2014, Astrophys. Space Sci., 350, 733
Takisa, P. M., Maharaj, S. D., & Ray, S. 2014, Astrophys. Space Sci., 354, 463
Takisa, P. M., Maharaj, S. D., & Mulangu, C. 2019, Pramana-J Phys, 92, 40
Thirukkanesh, S., & Ragel, F.C. 2013, Pramana C J. Phys., 81 , 275
Thirukkanesh, S., & Ragel, F. C. 2014, Astrophys. Space Sci., 354, 415
Thomas, V. O., Ratanpal, B. S., & Vinod kumar, P. C. 2005, Int. J. Mod. Phys. D, 14, 85
Tikekar, R., & Thomas, V. O. 2005, Pramana C J. Phys., 64, 5
Tikekar, R., & Jotania, K. 2009, Gravit. Cosmol., 15, 129
Witten, E. 1984, Phys. Rev. D, 30, 272
Usmani, A. A., et al. 2011, Phys. Lett. B, 701, 388
Vaidya,P. C., & Tikekar, R. 1982, J. Astrophys. Astron., 3, 325
Zeldovich, Y. B. 1962, Sov. Phys. JETP, 14, 1143